Retinal Cell Biology

Neuroretinal-Derived Caveolin-1 Promotes Endotoxin-Induced Inflammation in the Murine Retina

Jami M. Gurley,[1] Grzegorz B. Gmyrek,[1] Mark E. McClellan,[1] Elizabeth A. Hargis,[1] Stefanie M. Hauck,[2] Mikhail G. Dozmorov,[3] Jonathan D. Wren,[4] Daniel J. J. Carr,[1,5] and Michael H. Elliott[1]

[1]Department of Ophthalmology/Dean McGee Eye Institute, University of Oklahoma Health Sciences Center (OUHSC), Oklahoma City, Oklahoma, United States
[2]Research Unit Protein Science, Helmholtz Zentrum München, German Research Center for Environmental Health (GmbH), Munich, Germany
[3]Department of Biostatistics, Virginia Commonwealth University (VCU), Richmond, Virginia, United States
[4]Arthritis and Clinical Immunology Research Program, Division of Genomics and Data Sciences, Oklahoma Medical Research Foundation (OMRF), Oklahoma City, Oklahoma, United States
[5]Department of Microbiology and Immunology, University of Oklahoma Health Sciences Center (OUHSC), Oklahoma City, Oklahoma, United States

PURPOSE. The immune-privileged environment and complex organization of retinal tissue support the retina's essential role in visual function, yet confound inquiries into cell-specific inflammatory effects that lead to dysfunction and degeneration. Caveolin-1 (Cav1) is an integral membrane protein expressed in several retinal cell types and is implicated in immune regulation. However, whether Cav1 promotes or inhibits inflammatory processes in the retina (as well as in other tissues) remains unclear. Previously, we showed that global-Cav1 depletion resulted in reduced retinal inflammatory cytokine production but paradoxically elevated retinal immune cell infiltration. We hypothesized that these disparate responses are the result of differential cell-specific Cav1 functions in the retina.

METHODS. We used Cre/lox technology to deplete Cav1 specifically in the neural retinal (NR) compartment to clarify the role NR-specific Cav1 (NR-Cav1) in the retinal immune response to intravitreal inflammatory challenge induced by activation of Toll-like receptor-4 (TLR4). We used multiplex protein suspension array and flow cytometry to evaluate innate immune activation. Additionally, we used bioinformatics assessment of differentially expressed membrane-associated proteins to infer relationships between NR-Cav1 and immune response pathways.

RESULTS. NR-Cav1 depletion, which primarily affects Müller glia Cav1 expression, significantly altered immune response pathway regulators, decreased retinal inflammatory cytokine production, and reduced retinal immune cell infiltration in response to LPS-stimulated inflammatory induction.

CONCLUSIONS. Cav1 expression in the NR compartment *promotes* the innate TLR4-mediated retinal tissue immune response. Additionally, we have identified novel potential immune modulators differentially expressed with NR-Cav1 depletion. This study further clarifies the role of NR-Cav1 in retinal inflammation.

Keywords: caveolin-1, caveolin, caveolae, inflammation, neural retina, retina, retinal degeneration, immune response

Ocular inflammation promotes the development and progression of retinal degenerative diseases that lead to vision loss. Many of these retinal degenerative diseases, such as age-related macular degeneration, diabetic retinopathy, and glaucoma, are major causes of blindness and are strongly linked to dysregulated immune responses that damage retinal tissue and decrease visual function.[1]

The retina is a complex and delicate tissue that is highly susceptible to inflammation-mediated damage.[1,2] While the immune-privileged retina elicits immune responses when necessary, these responses are relatively suppressed by passive and active mechanisms intended to reduce inflammatory responses that lead to collateral damage.[3,4] Uncontrolled inflammatory activation or dysregulation of ocular immune suppression contributes to development and progression of retinal degeneration, retinal disease, and vision loss.[1] Unfortunately, the leading treatment option for dysregulated retinal inflammation is localized corticosteroid administration, which increases the risk for ocular conditions that exacerbate vision loss (e.g., cataracts, glaucoma). Therefore, understanding how to control chronic inflammation in the context of the immune-privileged retinal environment is important for developing novel therapeutics that

Investigative Ophthalmology & Visual Science

1

preserve retinal and visual function while minimizing off-target effects.

Several studies have implicated caveolin-1 (Cav1) as an established immune regulator in lung, brain, and myeloid-derived immune cells.[5–7] In most cell types, Cav1 is integrated into specialized plasma membrane domains called caveolae, which are involved in a variety of cellular processes including clathrin-independent endocytosis, endothelial transcytosis, lipid transport, vascular tone regulation, fibrosis, cell proliferation, monocyte/macrophage differentiation, and signaling pathway regulation.[6,8–15] Additionally, Cav1 and caveolar domains play complex roles in immune regulation with studies suggesting that Cav1 can either promote or inhibit inflammatory processes. For example, in the lung, Cav1 has been shown to *promote* inflammation by inhibiting endothelial nitric oxide synthase–dependent downregulation of proinflammatory cytokine production[6]; whereas, in macrophages, Cav1 *inhibits* TLR4 (Toll-like receptor 4)-mediated inflammatory stimulation via caveolae-dependent sequestration, which prevents receptor complex formation and downstream signaling.[10] Importantly, this suggests that such differences are due to distinct cell-specific Cav1-dependent functions.

In the retina, Cav1 is involved in important visual processes such as phagolysosomal digestion of photoreceptor outer segments by the retinal pigment epithelium (RPE),[16] maintenance of retinal vascular blood-retinal-barrier integrity,[17–20] and retinal neovascularization.[21] We and others have also implicated Cav1 function in retinal inflammation and immune response modulation.[22–24] However, the precise immunomodulatory role for Cav1 in retinal tissue is as perplexing as it appears to be in extraocular tissues, and has only begun to be investigated.[22] Previously, we showed that global-Cav1 deletion resulted in suppression of endotoxin-mediated retinal inflammatory cytokine production suggesting that Cav1 *promotes* retinal inflammatory activation.[22] Surprisingly, global Cav1 deletion paradoxically enhanced retinal immune cell infiltration implying that Cav1 function *suppresses* the immune response. Because Cav1 is expressed in several retinal cell populations, we reasoned that these paradoxical phenotypes could be explained by differential cell-specific Cav1 functions in the retina.

As our overall goal is to better understand the role of Cav1 in retinal degenerative processes that involve chronic retinal immune overactivation, the aim of this study was to identify the Cav1-expressing retinal compartment responsible for *promotion* of endotoxin-induced inflammatory responses. Here, we show that depletion of neural retinal-derived Cav1 (NR-Cav1) alone is sufficient to suppress inflammatory processes in the retina. Thus our work elucidates a specified role for NR-Cav1 in immune *activation* and contributes to our understanding of complex cell-specific Cav1 functions. Furthermore, this work emphasizes the importance of understanding protein function in cell-specific contexts and underscores the need for cell-specific targeting considerations during development of therapeutic interventions aimed at suppressing chronic retinal inflammation.

METHODS

Animals

NR-specific Cav1 KO mice (*Chx10*-Cre; Cav1[flox/flox]) were generated using Cre-Lox technology.[25] Animals carrying

Chx10-promoter-driven Cre recombinase (stock no. 005105; The Jackson Laboratory, Bar Harbor, ME, USA) were bred with animals carrying the Cav1 gene flanked by Lox P sites located upstream and downstream of exon 2.[26] Endothelial-specific Cav1 knock-out mice (Tie2-Cre; Cav1[flox/flox]) were generated similarly, using endothelial cell–specific recombination (B6.Cg-Tg (Tek-cre) 1Ywa/J; stock no. 008863; The Jackson Laboratory).[27] Cre-negative littermates were used as controls. Mice were screened for rd1 and rd8 mutations before this study. All procedures were approved by the University of Oklahoma Health Sciences Center Institutional Animal Care and Use Committee and comply with the Association for Research in Vision and Ophthalmology Statement for the Use of Animals in Ophthalmic and Visual Research.

Whole Retinal Tissue Lysis

Total retinal protein was obtained via whole retinal tissue lysis by brief sonication in ×2 lysis buffer (120 mM octyl glucoside, 2% Triton X-100, 20 mM Tris-HCl, pH 7.4, 200 mM NaCl, 1 mM EDTA) containing a protease inhibitor cocktail (Roche). Lysates were cleared by centrifugation at 13,000 rpm, at 4°C. Protein concentration was determined via BCA assay (ThermoSci, Cat no. 23225) and samples were diluted in ×6 Laemmli buffer.

Western Blotting

Retinas were homogenized in buffer containing 100 mM sodium carbonate and 1 mM EDTA using a plastic pellet pestle and brief pulse sonication on ice. Membranes were isolated by centrifugation at 16,000*g* in a benchtop microcentrifuge and membrane pellets were lysed in 1X lysis buffer. Protein content of lysates was determined by the BCA assay with bovine serum albumin as the standard. Protein separation was achieved via SDS-PAGE and proteins were transferred to nitrocellulose for immunoblotting with the following primary antibody dilutions: rabbit monoclonal anti–Caveolin-1 (1:1000; Cell Signaling no. 3267), mouse monoclonal anti–Actin (1:1000; no. MA1-744; ThermoFisher, St. Louis, MO, USA), rabbit polyclonal anti-TRAF3 (TNF Receptor-Associated Factor 3; 1:500; no. NBP-88639; Novus Biologicals, Littleton, CO, USA), and rabbit polyclonal anti-Gαt (Transducin; 1:4000; Santa Cruz Biotechnology, Dallas, TX, USA). Immunoreactivity was detected using species-appropriate horseradish peroxidase (HRP)–conjugated secondary antibodies (1:5000; GE Healthcare, Cleveland, OH, USA). Western blots were imaged via HRP chemiluminescent detection (Azure Biosystems, Inc., Dublin, CA, USA) and densitometric analyses were performed using Image Studio Lite software (LI-COR Biosciences, Lincoln, NE, USA).

Immunohistochemistry and Confocal Microscopy

Whole eye globes from euthanized adult mice were fixed in Prefer fixative (Anatech, Ltd., Battlefield, MI, USA), embedded in paraffin, and cut into 5-μm sections. Sections were deparaffinized, permeabilized with 1% Triton X-100 in PBS, then incubated with blocking solution (10% normal horse serum, 0.1% Triton X-100, in PBS) for one hour before immunohistochemistry, which was performed as previously described[28,29] using either hematoxylin and eosin (H&E) staining or the following antibodies: rabbit monoclonal anti-Caveolin-1 (1:100, no. 3267; Cell Signaling

Investigative Ophthalmology & Visual Science

Technology, Danvers, MA, USA); mouse monoclonal anti-glutamine synthetase (for Müller glia-specific marker; 1:5000 no. MAB302, clone GS-6; Millipore, Burlington, MA, USA); goat polyclonal anti-Brn3a (for retinal ganglion cell marker, 1:100; no. sc-31984; Santa Cruz Biotechnology); sheep polyclonal anti-Chx10 (for bipolar cell marker; 1:100; no. X1179P; Exalpha Biologicals Inc., Shirley, MA, USA); mouse monoclonal anti-opsin (for rod photoreceptor marker; 1:1000, no. O4886; Millipore), and rat monoclonal anti-mouse CD31 (for endothelial-specific marker; 1:100, no. DIA-310; Dianova International, Barcelona, Spain). Before immunohistochemistry, antigen retrieval, which consisted of boiling slides at 95°C for 20 minutes in 10 mM sodium citrate, was performed on slides stained with Brn3a or Chx10. Immunoreactivity was detected with Alexa Fluor-conjugated secondary antibodies (1:500; Life Technologies, Grand Island, NY, USA) or FITC-conjugated goat anti-mouse albumin (1:100, no. A90-234F; Bethyl Labs, Montgomery, TX, USA), and nuclei were stained with DAPI (4,6-diamidino-2-phenylindole). Images of immunostained retinal tissue sections were acquired on an Olympus FV1200 laser scanning confocal system using FluoView software (Olympus, Tokyo, Japan). Pseudocolors were assigned to images as follows: glutamine synthetase, Brn3a, Chx10, or 1D4 (green); Cav-1 (red); and nuclei (blue).

Optokinetic Tracking (OKT)

Visual acuity was assessed via noninvasive observations of behavioral (head turning) responses to a rotating visual gradient of different spatial frequencies in unrestrained mice in order to determine visual thresholds (OptoMotry; Dianova International).[30]

Electroretinography (ERG)

ERGs were recorded as described previously.[16,31] Briefly, overnight dark-adapted mice were anesthetized with ketamine (100 mg/kg) and xylazine (10 mg/kg), pupils were dilated with 0.5% atropine and 2.5% phenylephrine, gold wire electrodes were positioned on corneas, a reference electrode was placed inside the mouth, and a ground electrode was places in the tail. Rod-driven responses were assessed by presenting increasing scotopic stimuli (-3.7 to 2.6 log scotopic candela (cd) • s/m^2) via a Colordome Espion ERG recording system (Diagnosys, Lowell, MA, USA). Intensity response relationships for a- and b-wave were fit using the GraphPad Prism Michaelis-Menten equation in order to calculate maximum amplitudes.[16,31]

Mass Spectrometry-Based Proteomics

Membrane proteins were prepared from whole frozen retinal tissue as described previously.[23] Briefly, retinal tissues were lysed in high salt buffer (2M NaCl, 10 mM HEPES-NaOH, pH 7.4, 1 mM EDTA, complete protease inhibitors). Pellets were harvested via high-speed centrifugation and were subsequently homogenized in carbonate buffer (0.1 M Na$_2$CO$_3$, pH 11.3, 1 mM EDTA, complete protease inhibitors). Pellets were collected and re-extracted with carbonate buffer a second time. Pellets were collected and rehomogenized in urea buffer (4 M urea, 100 mM NaCl, 10 mM HEPES/NaOH, PH 7.4, 1 mM EDTA, complete protease inhibitors). The resulting membrane fractions were collected via centrifugation and were used for tryptic digest as described previously.[23] Label-free mass spectrometry was used to measure peptide abundances from membrane-enriched fractions of retinal samples from both NR-Cav1 WT and NR-Cav1 KO mice. For an in-depth description of the LC-MSMS procedure and detailed label-free peptide quantification analysis parameters, please refer to Hauck, et al.[23] Briefly, peptide spectra obtained by LC-MSMS on an Ultimate3000 nano HPLC system (Dionex, Sunnyvale, CA, USA) online coupled to a LTQ OrbitrapXL mass spectrometer (Thermo Fisher Scientific) were transformed to peak lists using Progenesis software, followed by label-free quantification based on peak intensities. Total list of identified peptides and proteins are available in *Supporting Information* (Supplemental Table S1). The mass spectrometry data have been deposited to the ProteomeXchange Consortium via the PRIDE[32] partner repository with the dataset identifier PXD016872 and 10.6019/PXD016872. Reviewer account details: Username: reviewer96885@ebi.ac.uk Password: VbXalKFX

Bioinformatics

Peptide abundances were log2-transformed and analyzed for differential abundance using the *limma* R package. The row-scaled abundances of the top 70 differentially expressed retinal proteins affected by NR-Cav1 depletion were visualized as a heatmap using the *pheatmap* R package (blue = downregulated; red = upregulated). The resulting complete proteomics data set was analyzed using both pathway and network analyses. KEGG (Kyoto Encyclopedia of Genes and Genomes) analysis and IPA (Ingenuity Pathway Analysis) were used for pathway enrichment to identify known gene sets affected by NR-Cav1 depletion. We obtained the protein-protein interaction (PPI) information for the most significantly changed proteins (adjusted P value ≤ 0.10) from the STRING v10 database.[33] Single PPIs (nodes with only one edge) were removed to reduce clutter and to focus upon *shared* PPIs within this network, and visualized with Cytoscape 3.7.[34] ShinyGO gene ontology analysis of all 177 significantly upregulated and 109 significantly downregulated proteins, respectively, was used to identify immune response related gene sets affected by NR-Cav1 depletion.[35]

Endotoxin-Induced Uveitis Model

Local, intravitreal injection of 1 μg LPS (*Salmonella typhimurium*; Sigma) was used to induce ocular inflammation as previously described.[22,36] Mice were anesthetized via intraperitoneal injection of ketamine (100 mg/kg)/xylazine (10 mg/kg). Each eye was then injected with either 1 μL LPS diluted in sterile PBS vehicle or PBS alone using a 10 μL glass syringe (Hamilton Company, Reno, NV, USA).

Cytokine/Chemokine Quantification Assay

Retinas from euthanized animals were collected 24 hours after LPS or PBS injection. Retinal tissue dissection was performed using a stereo dissecting microscope (Zeiss Stemi DV4; Carl Zeiss Microscopy, Jena, Germany). Retinas were processed and cytokines protein levels were measured by BioPlex suspension array (Bio-Rad Life Science, Hercules, CA, USA) as previously described.[22]

Flow Cytometry

Flow cytometry was performed on retinal samples as described previously for neural tissues with minor

modification.[22,37] Twenty-four hours after LPS or PBS injection, mice were perfused with PBS, and single-cell suspensions were obtained from retinas by digestion of minced tissue with liberase TL in RPMI 1640 at 37°C for 30 minutes. Next, the cell suspensions were passed through a 40-µm nylon cell strainer (Thermo Fisher Scientific), followed by washing with staining buffer (SB; PBS supplemented with 2% FBS, and 2 mM EDTA). Samples were blocked with anti-mouse CD16/32 (Fc-block; Invitrogen, San Jose, CA, USA) for 10 minutes at 4°C followed by staining with antibody cocktail containing Pacific-Blue-conjugated anti-mouse CD45 (clone 30-F11; Biolegend, San Diego, CA, USA), PE-conjugated anti-mouse Ly-6G/Ly6C (Gr-1) (clone RB6-8C5; Biolegend), APC-conjugated anti-mouse F4/80 (clone BM8; Biolegend), PE-Cy7-conjugated CD11b (clone M1/70; Biolegend), APC-Cy7-conjugated anti-mouse MHC II (clone M5/114.15.2, Biolegend), BV421-conjugated anti-mouse CCR2 (clone SA203G11, Biolegend), FITC-conjugated anti-mouse Ly6G (clone 1A8; Biolegend), and PE-conjugated anti-mouse Ly6C (clone HK1.4, Biolegend). Samples were incubated 20 minutes at 4°C and then washed with SB buffer. The data were acquired immediately after staining using a MacsQuant flow cytometer (Miltenyi Biotec, Auburn, CA USA). The events were gated by forward and side scatter, as well as sequential gating to distinguish subpopulation of infiltrating myeloid cells, similar like it was published elsewhere.[38] The exported FCS files were analyzed using FlowJo. If necessary, the values on compensation matrix were adjusted post acquisition using FlowJo, and the data on the flow graph were converted to Biex format (which displays linear around zero and log further out).

RESULTS

Neural Retinal Depletion of CAV1 Protein in Retinal Tissue

Our previously published results presented seemingly contradictory data where global-Cav1 depletion resulted in suppression of retinal inflammatory cytokine production with a concurrent elevation in retinal immune cell infiltration.[22] Because we hypothesized that this paradoxical result was due to distinct cell-specific Cav1 functions in different retinal cell populations, we aimed to separate potential cell-specific Cav1 effects using our conditional *Chx10*-Cre/Cav1^flox/flox neural retinal knockout animals (NR-Cav1 KO).[25,26,39] This model expresses Cre recombinase in neuroretinal progenitors during retinal development and results in Cav1 gene recombination in retinal neurons and Müller glia but not in other retinal cell types (i.e., astrocytes, microglia, RPE, or vascular cells) (Fig. 1A).[25] To validate Cav1 recombination in the retina, we first assessed CAV1 protein expression (via Western blot) in various tissues collected from NR-Cav1 wild type (WT) and KO animals (Fig. 1). Whole retinal tissue lysates from NR-Cav1 KO animals displayed a ~76% reduction of CAV1 protein compared to their WT counterparts suggesting that *Chx10*-Cre recombination results in significant depletion of whole retinal Cav1 expression. Residual CAV1 protein expression is likely primarily due to the remaining CAV1 protein expression in nontargeted retinal cell populations (e.g., retinal vascular cells), as well as some modest contribution from mosaic recombination in the neural retina.[40] There was no genotype-dependent difference in CAV1 protein expression
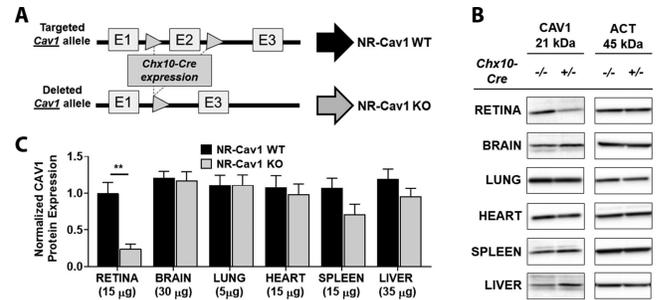
FIGURE 1. Effect of neuroretinal-specific deletion on whole retinal tissue CAV1 protein expression (*Chx10*-Cre/Cav1-flox model). (**A**) Schematic diagram illustrating the strategy for neuroretinal-specific *Cav1* deletion via *Chx10*-promoter driven Cre-mediated recombination of the floxed *Cav1* gene. (**B**) Representative Western blots of whole cell lysates from various tissues showing retina-specific CAV1 protein reduction following *Chx10*-Cre expression in the floxed *Cav1* model. Protein loads ranged from 5 µg to 35 µg, depending on tissue, to detect protein within the linear range of the assay. (**C**) Histogram of Western blot protein densitometry data quantification shows retinal tissue specific CAV1 protein reduction after NR-*Cav1*-depletion in *Chx*10-Cre/Cav1^+/+ mice compared to *Chx10*-Cre/Cav^−/− controls. β-actin was used as a loading control and for normalization. Data are mean ± SEM and were analyzed via Student's t-test (** $P < 0.01$; N = 7). ACT = β-actin.

in the other tissues we assessed (brain, lung, heart, spleen, or liver) (Figs. 1B, 1C).

Neural Retinal-Cav1 Depletion Primarily Targets Retinal Müller Glia

To ensure that our model specifically targeted Cav1 in the neural retinal compartment, we assessed CAV1 protein expression in retinal tissue sections by immunohistochemistry. To evaluate cell populations targeted by *Chx10*-mediated Cav1 depletion, we co-stained retinal tissue sections with cell-specific markers as follows: Müller glia, glutamine synthetase (GS); retinal ganglion cells (RGCs), Brain-Specific Homeobox/POU Domain Protein 3A (Brn3a); bipolar cells (BPCs), visual system homeobox 2 (Vsx2/Chx10); and rod photoreceptor cells (PRCs), opsin (Ret-P1) (Fig. 2, Supplementary Fig. S2). We observed the highest levels of CAV1 protein expression in Müller glia cells and retinal blood vessels, which agrees with previous studies.[17,23,25,41,42] In retinal tissue sections, Müller glia have a unique morphology where their cellular processes span the retina from the inner limiting membrane at the edge of the RGC layer to the external limiting membrane at the edge of the outer nuclear layer (ONL); whereas the retinal vasculature appears as discrete vessel cross-sections in the synaptic plexiform layers of the retina (Fig. 2, arrowheads). In Müller glia, colocalization of CAV1 with Müller marker GS was most prominent in areas surrounding the deep retinal blood vessels and in Müller apical processes spanning from Müller somata to the external limiting membrane (Fig. 2, white arrows). Importantly, CAV1 expression in the retinal vasculature was not affected by NR-Cav1 depletion (Fig. 2, arrowheads; Supplementary Fig. S2). Whereas, CAV1 staining in the Müller glia was largely ablated. Although, we did observe modest mosaicism (Fig. 2, black arrow) as previously reported.[40] Alternatively, RGCs of the inner retina did not express high levels of CAV1 (Supplementary Fig. S2A), nor did BPCs located in the inner nuclear layer
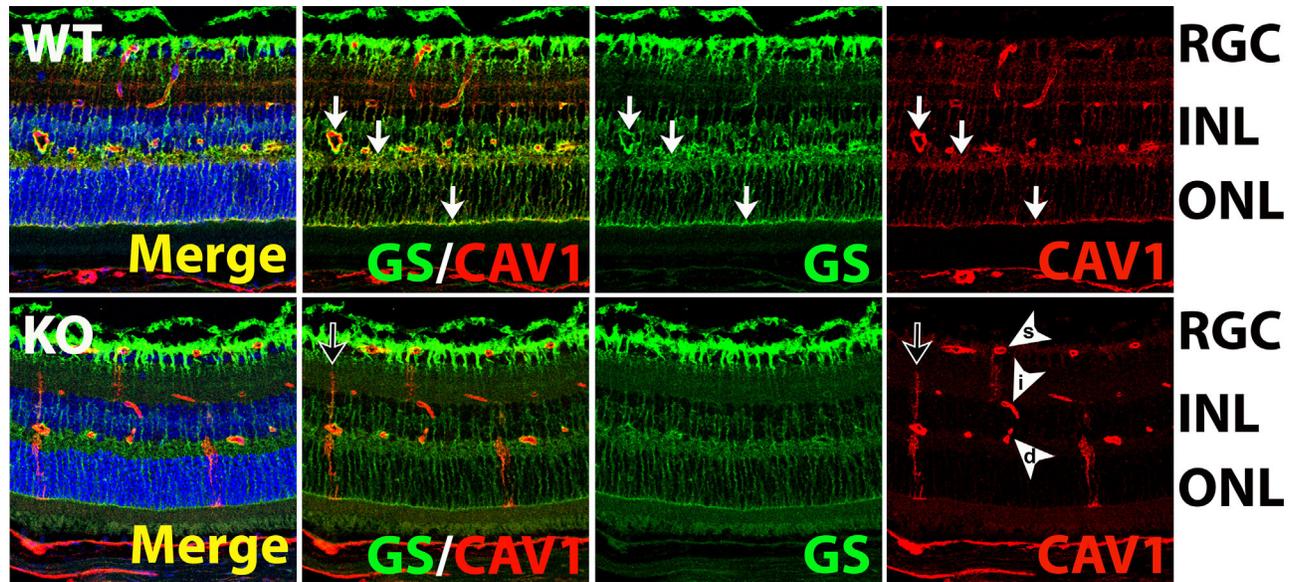
FIGURE 2. Neuroretinal-specific *Cav1* depletion targets retinal Müller glial cells. Immunohistochemical staining of mouse retinal sections stained with anti-CAV1 and costained with Müller cell-specific marker GS shows high Müller glial CAV1 protein expression and colocalization in cell regions associating with blood vessels, within Müller somata, and in apical processes near the external limiting membrane (*white arrows*). Blood vessel cross-sections representing the three layers of retinal vasculature also exhibit high levels of *CAV1* protein expression, but are not targeted by the NR-Cav1 KO model (*white arrowheads*; s, i, d = superficial, intermediate, and deep retinal blood vessels, respectively). Sparse mosaic Cre-mediated recombination results in occasional residual Müller glial CAV1 expression (*black arrows*). WT, NR-Cav1 WT; KO, NR-Cav1 KO; INL, inner nuclear layer.

(INL; Supplementary Fig. S2B). We detected only minimal CAV1 immunoreactivity in the ONL region, where retinal photoreceptors reside but this signal overlaps with Müller glial labeling (Supplementary Fig. S2C).[43] Thus our data support that CAV1 protein is most highly expressed in the Müller glia and blood vasculature of the mouse retina. This supports that the majority of CAV1 protein depletion observed in our retinal lysates (Fig. 1) was due to Müller-derived Cav1 recombination. Thus our NR-Cav1 KO provides an ideal model to assess the contribution of neural retinal Cav1 on the retinal immune response.

Neural Retinal-Cav1 Depletion Affects Immune-Related Protein Levels in Retinal Membrane Fractions

CAV1 protein is primarily localized to the cell membrane where it participates in formation and stabilization of specialized lipid raft domains, which facilitate regulatory effects on membrane receptor localization and activation.[44] Thus because Cav1 has been shown to regulate immune pathways at the level of membrane receptor complex formation, we reasoned that NR-Cav1 (likely Müller Cav1) could affect immune-related NR cell processes at the cell membrane. To assess whether depletion of NR-Cav1 was sufficient to alter membrane fraction composition in a way that could affect immune signaling we performed mass spectrometry and quantitative proteomics analysis on isolated retinal Cav1-associated membrane fractions from whole retinal tissue using previously described methods.[23] Our data showed significant downregulation of 109 proteins (including Cav1) and upregulation of 177 proteins in reti-

nal membrane fractions in response to NR-Cav1 deletion (Supplementary Table S1). Relative protein abundance data for the top 70 differentially expressed proteins are represented in Fig. 3 (blue = downregulated; red = upregulated). Retinas from our NR-Cav1 KO animals exhibited 70% reduction in CAV1 peptide abundance (Fig. 3; Supplementary Table S1), which agrees with Western blot validation data provided in Supplementary Figure S3 and is consistent with the 76% CAV1 reduction observed in whole retinal tissue lysates (Fig. 1). Collectively, our data suggest that the majority of retinal CAV1 protein resides within the plasma membrane compartment of neural retinal cell populations (i.e., primarily in Müller glia; Figs. 1–3). Altered retinal immune regulation resulting from NR-Cav1 depletion could be due to either downregulation or upregulation of immune effectors at the plasma membrane. To determine if NR-Cav1 influenced membrane compartmentalization of immune-related proteins, we used the online ShinyGO gene ontology (GO) enrichment analysis software to determine whether the downregulated or upregulated proteins contained known immune-regulatory functional groups.[35] Interestingly, 23 of the 109 genes for our downregulated proteins were found to be functionally associated with six distinct immune or stress response pathways (Table 1). Moreover, 46 of the 177 genes for our upregulated proteins were associated with the same 6 pathways (Table 2). Immune-related functional GO proteins that were downregulated included DDX21, MTHFD1, and ACHY, which support DNA synthesis and/or transcriptional processes. Other immune-related proteins in this group are known to influence membrane dynamics (SLC4A1, SGPL1) or contribute to cytoskeletal construction (KRT1). Additional stress response proteins downregulated in retinal membrane fractions largely consisted

TABLE 1. Effect of Neuroretinal-Specific Depletion on Immune-Related Gene Ontology Categories for Significantly Downregulated Genes Determined by Proteomics Data: Enrichment Analysis for All 109 Significantly Downregulated Genes After NR-Cav1 Depletion

N	High Level Go Category	Genes
23	Response to stress	PLEC SLC38A3 IDH1 SLC2A1 RAF1 BCAP31 CAV1 CAD H13 DDX21 NDUFB4 UBXN4 STT3B DNM2 KRT1 ABAT MT-ND4 MT-CYTB MAPKAP1 SLC4A1 ALDH3A2 PYCR2 AHCY
8	Immune system process	CAV1 DDX21 KRT1 RAF1 SGPL1 MTHFD1 SLC4A1 AHCY
4	Immune response	CAV1 DDX21 KRT1 AHCY
4	Regulation of immune system process	CAV1 KRT1 DDX21 SLC4A1
2	Activation of immune response	CAV1 KRT1
2	Immune effector process	DDX21 KRT1

ShinyGO analysis was performed on all 109 genes that were identified by proteomics as being significantly downregulated following NR-Cav1 depletion. Table represents immune-associated functional category groups ("High level GO category") defined by high-level gene ontology terms used by ShinyGO analysis software. Table also includes both the number ("N") and gene names ("Gene") for downregulated genes identified to contribute to the immune-associated GO categories.

TABLE 2. Effect of Neuroretinal-Specific Depletion on Immune-Related Gene Ontology Categories for Significantly Upregulated Genes Determined by Proteomics Data: Enrichment Analysis for All 177 Significantly Upregulated Genes After NR-Cav1 Depletion

N	High Level Go Category	Genes
45	Response to stress	DUSP3 RBM14 ANXA6 RAD21 HSPA9 ANXA5 VCP PCK2 H2AFX UBE2N ENTPD2 VAMP4 PPP3CA GSTM5 GORASP2 UCHL5 XAB2 TRAF3 OXCT1 DLG1 FEN1 CORO1B HSPD1 CAPN2 DDAH1 SFPQ NONO NEDD4 ADRA2A MACROD1 NPLOC4 SMC1A CORO2B HNRNPA1 USP14 PRKCA PRMT1 ANXA7 UCHL1 PTPN11 WDFY1 GSTM7 CAMK2G HSPA4L XRN2
17	Immune system process	DUSP3 RBM14 HSPD1 VAMP4 TRAF3 HSPA9 SFPQ NONO NPLOC4 USP14 RPS17 PRMT1 PTPN11 DLG1 NEDD4 WDFY1 UBE2N
13	Immune response	DUSP3 RBM14 VAMP4 TRAF3 SFPQ NONO NPLOC4 USP14 DLG1 NEDD4 WDFY1 HSPD1 UBE2N
12	Regulation of immune system process	DUSP3 RBM14 HSPD1 TRAF3 HSPA9 SFPQ NONO NPLOC4 PRMT1 DLG1 WDFY1 UBE2N
9	Activation of immune response	DUSP3 RBM14 SFPQ NONO NPLOC4 TRAF3 WDFY1 HSPD1 UBE2N
4	Immune effector process	TRAF3 NPLOC4 DLG1 HSPD1

ShinyGO analysis was performed on all 177 genes that were identified by proteomics as being significantly upregulated following NR-Cav1 depletion. Table represents immune-associated functional category groups ("High level GO category") defined by high-level gene ontology terms used by ShinyGO analysis software. Table also includes both the number ("N") and gene names ("Gene") for upregulated genes identified to contribute to the immune-associated GO categories.

of several metabolic mediators (SLC2A1, SLC38A3, IDH1, PYCR2, ALDH3A2, NDUFB4, MT-ND4, and MT-CYTB).

The 46 upregulated proteins associated with the 6 ShinyGO immune and/or stress response pathways (Table 1) included TRAF3 (TNF Receptor Associated Factor 3) and NPLOC4 (Nuclear Protein Localization protein 4 homolog), which were shown to participate in all six pathways. Interestingly, Traf3 is a known inflammatory regulator in nonretinal tissues that associates with immune receptor complexes at the cell membrane to modulate downstream signaling.[45–48] NPLOC4 and VCP (another identified upregulated protein) are known to participate in protein complex formation to facilitate immune receptor ubiquitination and proteosomal degradation.[49] USP14, UBE2N, UCHL1/5, and NEDD4 also play a role in ubiquitination of proteins, and NEDD4 has been show to stabilize TRAF3 via direct K63-ubiquitination.[50,51] Other upregulated proteins related to these immune or stress-related pathways included those involved in calcium responses or synaptic vesicle dynamics and neurotransmission regulation (PPP3CA, CAMK2G, ANXA6, ANXA7, DLG1, CAPN2, VAMP4, ENTPD2), receptor membrane localization (PRKCA), metabolic regulators (PCK2, OXCT1, GSTM5/7), transcriptional regulation (SFPQ, NONO, PRMT1, WDFY1, XAB2, XRN2), ERK-pathway regulation (DUSP3, PTPN11), and DNA/chromatin modification (H2AFX, RAD21, FEN1, SMC1A).

Neural Retinal-Cav1 Promotes Retinal Endotoxin-Mediated Immune Response

Our proteomics results suggested that NR-Cav1 depletion significantly altered immune-related retinal membrane-associated protein composition. To investigate whether NR-Cav1 affects the retinal innate immune response, we used our NR-Cav1 KO model to assess whole retinal cytokine levels after ocular immune challenge via intravitreal LPS injection (Fig. 4). Immune induction resulted in a robust proinflammatory cytokine response in WT animals (Fig. 4, LPS effect = *). Similar to our previous data collected from global-Cav1-KO retinas,[22] whole retinal tissue from LPS-treated NR-Cav1 KO animals exhibited lower inflammatory cytokine concentrations (pg/mL) than their WT counterparts (Fig. 4: IL-6 [interleukin 6]: *28.3%*, 165.5 NR-KO vs 585.4 NR-WT; CXCL1/KC [C-X-C motif chemokine ligand 1]: 18.1%, 792.0 NR-KO vs 4,374.0 NR-WT; CCL2/MCP-1 [monocyte chemoattractant protein 1]: *22.2%* 185.9 NR-KO vs 838.4 NR-WT; and IL-1β [interleukin 1 beta]: *71.3%*, 15.9 NR-KO vs 22.3 NR-WT). These data suggest that NR-derived Cav1 promotes LPS-induced retinal immune activation. Furthermore, these findings suggest that the suppressive effect on cytokine/chemokine release previously observed in global-Cav1 KO animals was likely due to NR-Cav1 depletion.[22]
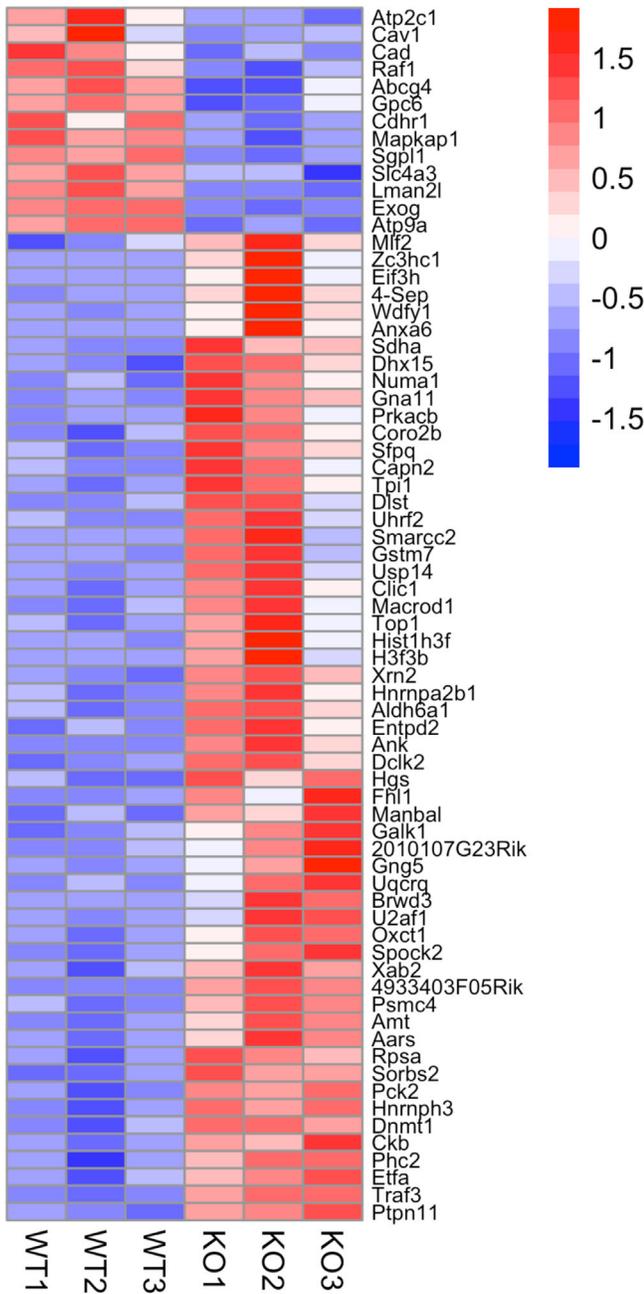
FIGURE 3. Effect of neuroretinal-specific depletion on membrane-associated protein composition. Mass spectrometry-based proteomics heat map analysis (*pheatmap* R) of membrane raft fractions from whole retinal tissue. Each replicate sample contained pooled retinas from eight mice. *Blue* = downregulated; *red* = upregulated. Heatmap represents peptide abundance quantification for the top 70 differentially expressed peptides as a result of NR-Cav1 depletion. Data are mean ± SEM and were analyzed via Student's *t*-test (* *P* < 0.05; *** *P* < 0.001).

FIGURE 4. Neuroretinal-specific Cav1 depletion blunts endotoxin-mediated retinal proinflammatory cytokine production. Multiplex protein suspension array analysis showing endotoxin-mediated inflammatory activation in retinas from *Chx10*-Cav1 WT and KO animals 24 hours after intravitreal LPS injection. Histograms represent measured concentrations of proinflammatory cytokines/chemokines (**A**) IL-6, (**B**) CXCL1/KC, (**C**) CCL2/MCP-1, and (**D**) IL-1β. Data are mean ± SEM and were analyzed using two-way analysis of variance, with Fisher's LSD post-hoc. Treatment effect: *$P < 0.05$, ***$P < 0.001$, ****$P < 0.0001$; Genotype effect: ††$P < 0.01$, †††$P < 0.001$. CXCL1/KC, C-X-C motif chemokine ligand 1; CCL2/MCP-1, monocyte chemoattractant protein 1; IL-1β, interleukin 1 beta.

by differential Cav1 functions in the neuroretina versus the vascular endothelium. Thus we hypothesized that we would observe *reduced* immune cell infiltration in the NR-Cav1 KO model following intraocular LPS challenge because vascular Cav1 is unperturbed. As expected, using our previous flow cytometry strategy, we found that NR-Cav1 KO animals exhibited lower levels of retinal immune cell infiltrate than controls following LPS challenge (CD45$^+$, "total leukocytes": 23.2%, 20,354 NR-KO vs. 4,713 NR-WT; CD45$^+$F4/80$^-$GR1$^+$, "polymorphonuclear leukocytes" ("PMNs"): 22.1%, 4325 NR-KO vs. 19,596 NR-WT; CD45$^+$F4/80$^+$GR1$^+$, "inflammatory monocytes": 52.9% 202 NR-KO vs. 382 NR-WT; and CD45$^+$F4/80$^+$GR1$^-$, "macrophages" ("MΦs"): 58.7%, 311 NR-KO vs. 530 NR-WT) (Fig. 5). Direct comparison of these data new data with our previous global-Cav1 KO results further suggests that NR-Cav1 promotes the retinal innate immune response to LPS, and that NR-Cav1 depletion is sufficient to prevent both proinflammatory cytokine production *and* immune cell infiltration into retinal tissue. To further validate that this observation was due to cell context-specific effects, we similarly assessed immune infiltration in endothelium-specific Cav1 KO animals (*Tie2*-Cre Cav1 KO model; Endo-Cav1 KO), which have previously been shown to exhibit efficient depletion of Cav1 in vascular endothelia.[27,52–55] As shown in Supplementary Figure S4, Tie2-cre efficiently depletes Cav1 from the retinal vasculature

Previously, in global-Cav1 KO animals, we made the paradoxical observation that although cytokines/chemokines were suppressed, immune cell infiltration into the retina following LPS stimulation was *elevated* compared to WT mice.[22] As Cav1 plays roles in several cell processes and is expressed in multiple retinal cell populations, we reasoned that the elevated immune cell infiltrate could be explained
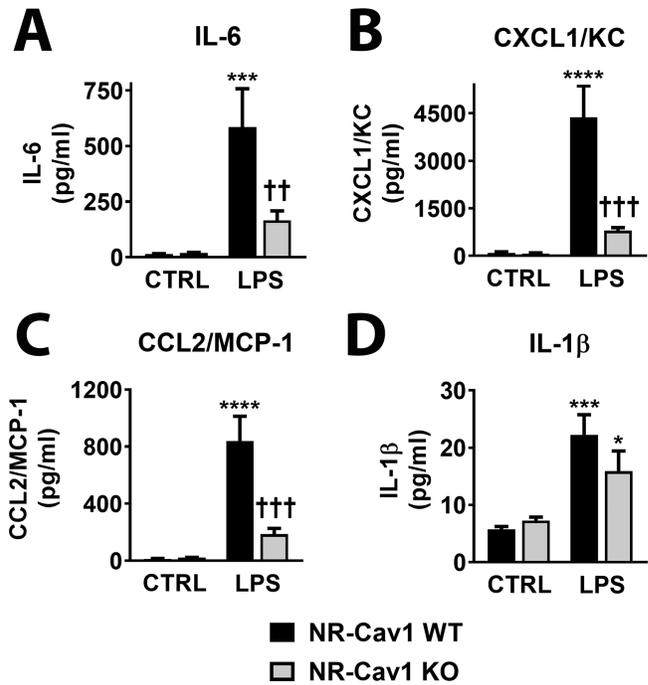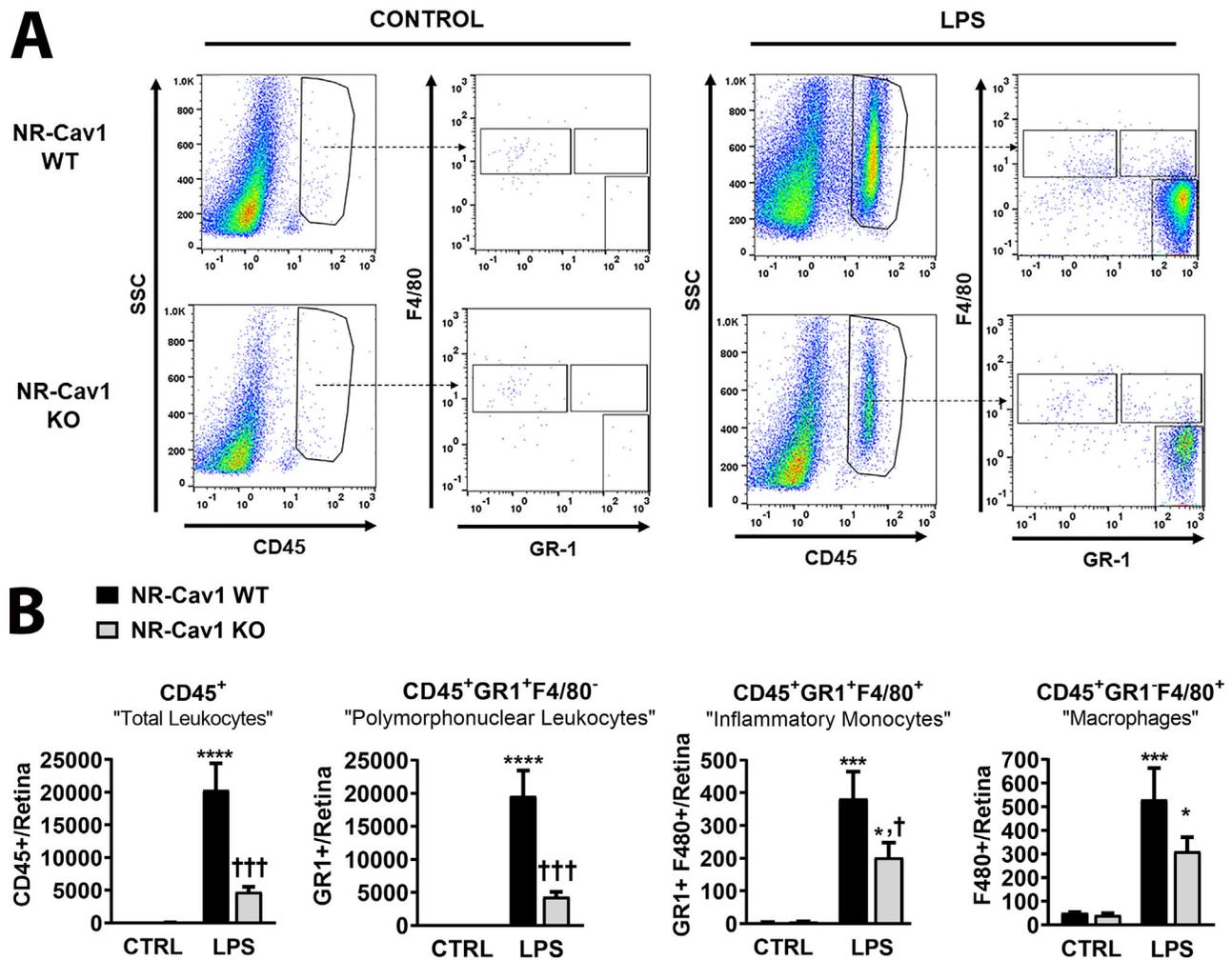
FIGURE 5. Neuroretinal-specific *Cav1* depletion reduces immune cell recruitment to retinal tissue. (**A**) Flow cytometry dot plots and (**B**) histogram quantifications representing immune cell infiltration into retinal tissue 24 hours after intraocular LPS challenge. Animals were perfused before collection of whole retinal tissue from *Chx10*-Cav1 WT and *Chx10*-Cav1 KO animals. Gating strategy represents the following cell populations: "total leukocytes" (CD45$^+$), "PMNs" (CD45$^+$F4/80$^-$/GR1$^+$), "inflammatory monocytes" (CD45$^+$F4/80$^+$/Gr1$^+$), and "macrophages/MΦ" (CD45$^+$F4/80$^+$/GR1$^-$). (**B**) Histogram quantification of flow cytometry data from control or LPS-treated *Chx10*-Cav1 WT and *Chx10*-Cav1 KO animals. Data are mean ± SEM and were analyzed using two-way analysis of variance, with Fisher's LSD post hoc. Treatment effect: $*P < 0.05$, $**P < 0.01$, $***P < 0.001$, $****P < 0.0001$; genotype effect: †$P < 0.05$, †††$P < 0.001$.

while leaving the NR-Cav1 unperturbed. Interestingly, Endo-Cav1 KO mice did not exhibit blunted infiltration, which further supports that NR-Cav1, specifically, plays a crucial role in retinal immune activation ("total leukocytes": 2741 NR-KO vs. 2435 NR-WT; "PMNs": 2164 NR-KO vs. 1799 NR-WT; "inflammatory monocytes": *163* NR-KO vs. 184 NR-WT; and "MΦs": 445 NR-KO vs. 441 NR-WT) (Supplementary Fig. S5). In Figure 4 and Supplementary Figure S5, we used the same flow cytometry labeling strategy used in our previous study to directly compare NR- and Endo-Cav1 specific effects with our data from global-Cav1 KO animals.[22] However, further analysis showed that this labeling strategy results in cell heterogeneity within the CD45$^+$GR$^-$F4/80$^+$ population (Supplementary Fig. S6). To validate our NR-Cav1 KO findings of blunted immune cell infiltration and to gain additional insight into the identity of immune cells present, we subsequently used six-color flow cytometry to assess retinal immune

infiltrate in LPS-stimulated NR-Cav1 KO animals (Fig. 6). This new flow strategy showed a significant genotype-dependent decrease in LPS-stimulated "total myeloid cells" (CD45$^+$CD11b$^+$: 815 NR-KO vs 1343 NR-WT) and "granulocyte" (CD45^{int}CD11b$^+$MHCII$^-$CCR2$^-$Ly6G$^+$Ly6C$^-$: 98 NR-KO vs. 289 NR-WT) populations (Figs. 6A, 6C). Thus the primary infiltrating cell type affected by NR-Cav1 depletion at this time point after LPS stimulation is likely neutrophils; however, we cannot rule out the presence of other granulocyte populations. There was no genotype-dependent difference in "microglia" (CD45^{int}CD11b$^+$MHCII$^-$CCR2$^-$Ly6G$^-$Ly6C$^-$: 25 NR-KO vs. 29 NR-WT, Fig. 6B), "retinal myeloid cells" (CD45^{int}CD11b$^+$MHCII$^-$CCR2$^-$Ly6G$^-$Ly6C$^+$: 210 NR-KO vs. 222 NR-WT, Fig. 6B) or "Monocyte/MΦ" populations (CD45^{hi}CD11b$^+$MHCII$^-$CCR2$^-$Ly6G$^-$Ly6C$^+$: 98 NR-KO vs. 96 NR-WT, Fig. 6E; CD45^{hi}CD11b$^+$MHCII$^-$CCR2$^+$Ly6G$^-$Ly6C$^+$: 59 NR-KO
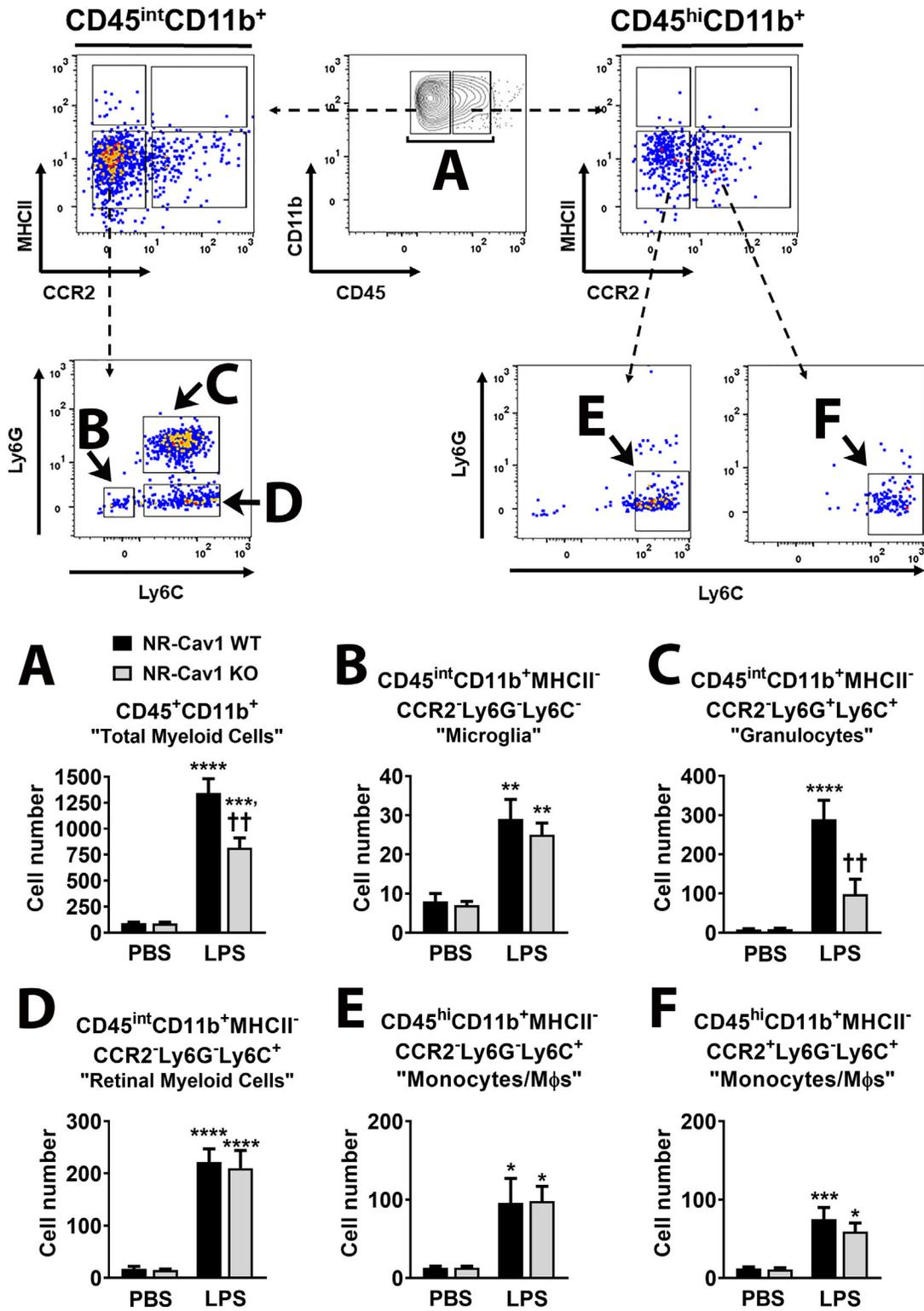
FIGURE 6. Validation of neuroretinal-specific depletion effects on retinal tissue immune cell recruitment using six-color flow cytometry. *Upper panel:* Representative dot plots from an LPS-treated NR-Cav1 WT retina and illustrates the gating strategy used for six-color flow cytometry. These data were obtained and analyzed with LPS-treated NR-Cav1 KO and PBS-treated NR-Cav1 WT and NR-Cav1 KO samples (representative dot plot for PBS samples is shown in Supplementary Figure S7). *Lower panel:* Corresponding histogram quantifications represent defined immune cell populations (**A–F**). Animals were perfused before collection of whole retinal tissue. Data represent all PBS-treated and LPS-treated NR-Cav1 WT and NR-Cav1 KO samples and are mean ± SEM. Data were analyzed via two-way analysis of variance with Tukey's post-hoc. Treatment effect: *$P < 0.05$, **$P < 0.01$, ***$P < 0.001$, ****$P < 0.0001$; Genotype effect: ††$P < 0.01$.

vs. 75 NR-WT, Fig. 6F) using this labeling approach. The discrepancy regarding significantly lower infiltrating CD45^{hi} monocytes with the three-color versus six-color flow cytometry protocols is likely due to more rigorous separation of monocyte populations with six-color flow cytometry (Fig. 5 vs. Fig. 6, Supplementary Fig. S7; also, see Supplementary Fig. S6).[56–62] To further assess potential effects of NR-Cav1 on retinal vessel leakage, we also used immunohistochemical staining of endogenous albumin in retinal tissue sections (Supplementary Fig. S8). Our data show that while Endo-Cav1 KO retinas exhibit staining of endogenous albumin in RGC, ONL, and choroidal tissue layers (Supplementary Fig. S8, white arrows), albumin was largely contained within the vascular lumen of superficial retinal vessels in NR-Cav1 KO retinas. This further supports that NR-Cav1 does not have a significant effect on vessel permeability.

Bioinformatics Assessment of Potential CAV1-TRAF3 Protein Interactions

Collectively, our suggested that NR-Cav1 plays a role in retinal immune regulation and several immune-regulated proteins were altered in our membrane fractions. Existing proteomics data sets suggest that Traf3 is highly expressed in the retina compared to other tissues (Genecards), However, Traf3 function in the retina has not been rigorously investigated. Thus we were interested in assessing possible interactions between TRAF3 and CAV1 in the context of retinal immune regulation. First, to validate our proteomics data, we identified upregulation of membrane TRAF3 in NR-Cav1 retinas using Western blot analysis (Fig. 3; Supplementary Fig. S3). To better understand how CAV1 might interact with TRAF3 to modulate retinal immune responses, we used the STRING v10 database to obtain protein-protein interaction (PPI) information for the most significantly changed proteins (adjusted P value ≤ 0.10) within our data set.[33] Supplementary Fig. S9 shows that CAV1 is known to share at least 19 PPIs with seven proteins and illustrates how loss of Cav1 might impact the activity and/or upregulation of 4 proteins (including TRAF3) (Fig. 3; Supplementary Fig. S9). At least 3 of the 4 CAV1-TRAF3 shared interacting proteins have been associated with TNF-alpha–induced cell death (i.e., RIPK1/Receptor-interacting serine/threonine-protein kinase 1, TRAF2/ tumor necrosis factor [TNF] receptor-associated factor 2, and TRADD/ tumor necrosis factor receptor type 1-associated DEATH domain protein).[63,64] The bulk of the PPIs shared with CAV1 are with TRAF3 and PTPN11 (tyrosine-protein phosphatase non-receptor type 11), which TRAF3 is known to inhibit. Many of these shared PPIs (e.g., EGF/epidermal growth factor, SRC/neuronal proto-oncogene tyrosine-protein kinase, BCAR1/breast cancer anti-estrogen resistance protein 1) are also associated with anoikis (programmed cell death on detachment from the extracellular matrix). Indeed, CAV1 is reported to increase resistance to anoikis, which may be related to Cav1's role in neuroprotection.[65,66] Because the changed proteins were not significantly enriched in immune functions or pathways with this analysis, we cannot rule out the possibility that the immune effects of Cav1 KO may be indirect and due to alterations in the structure of the plasma membrane. This may, in fact, reconcile why some studies observe a pro- or anti-inflammatory effect, because a change in membrane dynamics could affect both.

DISCUSSION

Cav1 has been shown to play a role in retinal immunity and, in retinal tissue, CAV1 protein is most highly expressed in the Müller glial population of the neural retina and the retinal vasculature (Fig. 2). Previous work from our laboratory showed that Cav1 depletion in global-Cav1 KO animals reduced retinal inflammatory cytokine production in response to LPS, which suggested that Cav1 *promotes* inflammation in retinal tissue.[22] Our current results determine that NR- Cav1 depletion is sufficient to produce this response (Fig. 4). Likewise, this work shows that NR-Cav1 depletion also blunts immune cell infiltration consistent with the effect on retinal cytokines/chemokines (Figs. 5, 6, Supplementary Fig. S7). However, previously, global-Cav1 KO animals exhibited a concurrent and paradoxical *elevation* in immune infiltrate suggesting that NR-Cav1 depletion was not responsible for this effect.[22] We initially hypothesized that the elevated immune cell infiltration in the global-Cav1 KO animals would be explained by enhanced vascular permeability due to endothelial *Cav1* depletion and expected to observe elevated immune cell infiltrate in the Endo-Cav1 KO model. Interestingly, we observed no differences in the number of immune cells between Endo-Cav1 KO and control animals. Thus, while we have shown here that Endo-Cav1 depletion does not blunt infiltration, it also does not explain the *elevated* infiltration observed in the global-Cav1 KOs.[22] We believe, rather, that immune cell-specific effects resulting from global-Cav1 KO depletion are likely responsible for the elevated infiltrate as our previous work showed that global-Cav1 KO animals harbor more CD45^{+} cells within retinal vasculature.[22] Neural retina-specific Cav1 depletion via Chx10-Cre does not target systemic or resident immune cell populations but depletes Cav1 from the major retinal macroglial population (Müller glia) making it ideal to examine the local impact of Cav1. Thus we suggest that the increased presence of circulating immune cells in global-Cav1 KO animals results in greater accessibility to retinal vessels under basal conditions and primes the retina for enhanced immune uptake following immune activation that induces vessel permeability. Alternatively, the enhanced infiltration phenotype observed in the global-Cav1 KO could be explained by an unknown mechanism due to loss of RPE-specific Cav1-dependent BRB functions, which are also not targeted in our NR-Cav1 KO animals. We plan to investigate these possibilities in future studies. Nevertheless, this study helps clarify the role of NR-Cav1 as a positive regulator of retinal inflammation via production of retinal inflammatory chemoattractants in response to LPS stimulation.

Our data support that the majority of NR-Cav1 protein resides within the Müller glial cell population, which is in agreement with ours and other previous work.[25] In addition to their important structural and neurosupportive roles in the retina (i.e., metabolic homeostasis, neurotransmitter recycling, and intercellular communication), Müller glia also play an important role in retinal immunity.[67,68] Müller glia express innate immune receptors, including TLR4 and CD40 and are capable of inflammatory and neuroprotective cytokine production.[68,69]

Intriguingly, Cav1 has been shown to be important for secretion of cytokines such as IL-6 in prostate cancer cells.[70,71] Furthermore, previous data from our lab suggests a Cav1-dependent role in retinal IL-6 family cytokine production that is upstream of neuroprotective signaling (via STAT3 pathway activation).[25] These studies are consistent with
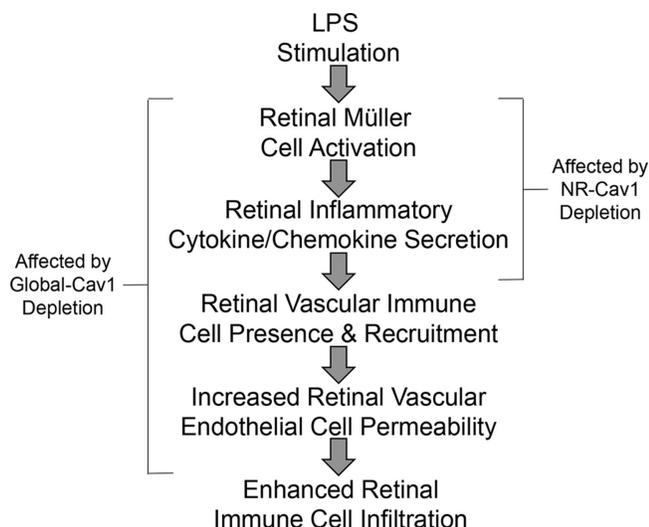
FIGURE 7. Simplified model summarizing retinal immune response following LPS challenge. A simple diagram summarizes the sequence of events after intravitreal immune challenge with LPS, which highlights events affected by NR-Cav1 depletion versus global-Cav1 depletion.

our current observation of blunted LPS-induced cytokine production in NR-Cav1 KO mice and support a role for Müller-derived inflammatory cytokine production and secretion in retinal immunity. Importantly, resident microglial cells in the retina express negligible levels of Cav1 and are not targeted by the NR-Cav1 model. Thus direct microglial responses to LPS are unlikely to be affected by NR-Cav1 depletion, which may explain the incomplete suppression of cytokine levels following immune induction (Fig. 4). Interestingly, it has been suggested that bidirectional inflammatory communication occurs between Müller cells and microglia.[72] It is therefore possible that NR-Cav1 depletion could secondarily affect the extent of microglial responses to injury, either through ablation of Müller-mediated amplification of microglial activation or potential contributions of Müller-derived effects on microglial function.[72–74] Hence, further studies are needed to fully understand the contribution of Müller glia-derived immune responses, interactions between Müller cells and microglia in the context of immune activation, and the role of Müller glia in maintenance of the retinal immune-privileged microenvironment.

Because Cav1 is known to stabilize cell surface receptors in specialized lipid raft membrane domains,[44] it is conceivable that the blunted immune activation observed in NR-Cav1 KO retinas was due to altered immune receptor complex formation and activation. Our findings suggest that NR-Cav1 depletion significantly changed retinal membrane composition; however, no difference in immune receptor abundance was detected. Excitingly, TRAF3, which is a known cytosolic regulator of immune receptor complexes, was found to be upregulated in NR-Cav1 KO retinal membrane fractions (Fig. 3, Supplementary S3, Supplementary S10). Remarkably, TRAF3 is highly expressed in retinal tissue, but its function is poorly understood. Additionally, Traf3 can directly interact with immune receptors, including CD40 and TLR4, which are both expressed in Müller glial cells.[75] As we believe that Traf3 may play a previously-unappreciated role in retinal inflammatory modulation, our

laboratory has recently developed NR-Traf3 KO animals, and these studies are currently in progress.

Our findings here show that NR-Cav1 ablation is sufficient to prevent retinal inflammatory induction in response to LPS-induced challenge (see Fig. 7). This underscores the importance for understanding cell-specific protein functions in disease. Specifically, this study suggests that NR-Cav1, NR-Cav1 regulators, or manipulation of NR-caveolae formation could serve as targets for chronic inflammatory suppression.[76] Our future studies include investigation of (1) further examination of Cav1-dependent roles of Müller glia in retinal immune regulation, (2) the role of Traf3 in retinal tissue function, and (3) potential interactions (direct or indirect) between Cav1 and Traf3.

References

1. Whitcup SM, Nussenblatt RB, Lightman SL, Hollander DA. Inflammation in retinal disease. *Int J Inflam*. 2013;2013:724648.
2. Murakami Y, Ishikawa K, Nakao S, Sonoda KH. Innate immune response in retinal homeostasis and inflammatory disorders. *Prog Retin Eye Res*. 2019;74:100778.
3. Streilein JW. Ocular immune privilege: the eye takes a dim but practical view of immunity and inflammation. *J Leukoc Biol*. 2003;74:179–185.
4. Zhou R, Caspi RR. Ocular immune privilege. *F1000 Biol Rep*. 2010;2:3.
5. Chidlow JH, Sessa WC. Caveolae, caveolins, and cavins: complex control of cellular signalling and inflammation. *Cardiovasc Res*. 2010;86:219–225.
6. Garrean S, Gao XP, Brovkovych V, et al. Caveolin-1 regulates NF-kappaB activation and lung inflammatory response to sepsis induced by lipopolysaccharide. *J Immunol*. 2006;177:4853–4860.
7. Blochet C, Buscemi L, Clement T, Gehri S, Badaut J, Hirt L. Involvement of caveolin-1 in neurovascular unit remodeling after stroke: Effects on neovascularization and astrogliosis. *J Cereb Blood Flow Metab*. 2020;40:163–176.
8. Drab M, Verkade P, Elger M, et al. Loss of caveolae, vascular dysfunction, and pulmonary defects in caveolin-1 gene-disrupted mice. *Science*. 2001;293:2449–2452.

9. Fu Y, Moore XL, Lee MK, et al. Caveolin-1 plays a critical role in the differentiation of monocytes into macrophages. *Arterioscler Thromb Vasc Biol*. 2012;32:e117–125.

10. Wang XM, Kim HP, Nakahira K, Ryter SW, Choi AM. The heme oxygenase-1/carbon monoxide pathway suppresses TLR4 signaling by regulating the interaction of TLR4 with caveolin-1. *J Immunol*. 2009;182:3809–3818.

11. Ghitescu L, Fixman A, Simionescu M, Simionescu N. Specific binding sites for albumin restricted to plasmalemmal vesicles of continuous capillary endothelium: receptor-mediated transcytosis. *J Cell Biol*. 1986;102:1304–1311.

12. Chaudhary KR, Cho WJ, Yang F, et al. Effect of ischemia reperfusion injury and epoxyeicosatrienoic acids on caveolin expression in mouse myocardium. *J Cardiovasc Pharmacol*. 2013;61:258–263.

13. Fernandez-Rojo MA, Gongora M, Fitzsimmons RL, et al. Caveolin-1 is necessary for hepatic oxidative lipid metabolism: evidence for crosstalk between caveolin-1 and bile acid signaling. *Cell Rep*. 2013;4:238–247.

14. Milici AJ, Watrous NE, Stukenbrok H, Palade GE. Transcytosis of albumin in capillary endothelium. *J Cell Biol*. 1987;105:2603–2612.

15. Zhao YY, Zhao YD, Mirza MK, et al. Persistent eNOS activation secondary to caveolin-1 deficiency induces pulmonary hypertension in mice and humans through PKG nitration. *J Clin Invest*. 2009;119:2009–2018.

16. Sethna S, Chamakkala T, Gu X, et al. Regulation of Phagolysosomal Digestion by Caveolin-1 of the Retinal Pigment Epithelium Is Essential for Vision. *J Biol Chem*. 2016;291:6494–6506.

17. Gu X, Fliesler SJ, Zhao YY, Stallcup WB, Cohen AW, Elliott MH. Loss of caveolin-1 causes blood-retinal barrier breakdown, venous enlargement, and mural cell alteration. *Am J Pathol*. 2014;184:541–555.

18. Chow BW, Gu C. Gradual Suppression of Transcytosis Governs Functional Blood-Retinal Barrier Formation. *Neuron*. 2017;93:1325–1333.e1323.

19. Klaassen I, Hughes JM, Vogels IM, Schalkwijk CG, Van Noorden CJ, Schlingemann RO. Altered expression of genes related to blood-retina barrier disruption in streptozotocin-induced diabetes. *Exp Eye Res*. 2009;89:4–15.

20. Wang Z, Liu CH, Huang S, et al. Wnt signaling activates MFSD2A to suppress vascular endothelial transcytosis and maintain blood-retinal barrier. *Sci Adv*. 2020;6:eaba7457.

21. Jiang Y, Lin X, Tang Z, et al. Critical role of caveolin-1 in ocular neovascularization and multitargeted antiangiogenic effects of cavtratin via JNK. *Proc Natl Acad Sci USA*. 2017;114:10737–10742.

22. Li X, Gu X, Boyce TM, et al. Caveolin-1 increases proinflammatory chemoattractants and blood-retinal barrier breakdown but decreases leukocyte recruitment in inflammation. *Invest Ophthalmol Vis Sci*. 2014;55:6224–6234.

23. Hauck SM, Dietter J, Kramer RL, et al. Deciphering membrane-associated molecular processes in target tissue of autoimmune uveitis by label-free quantitative mass spectrometry. *Mol Cell Proteomics*. 2010;9:2292–2305.

24. Cehofski LJ, Kruse A, Magnusdottir SO, et al. Dexamethasone intravitreal implant downregulates PDGFR-alpha and upregulates caveolin-1 in experimental branch retinal vein occlusion. *Exp Eye Res*. 2018;171:174–182.

25. Reagan A, Gu X, Hauck SM, et al. Retinal Caveolin-1 Modulates Neuroprotective Signaling. *Adv Exp Med Biol*. 2016;854:411–418.

26. Cao G, Yang G, Timme TL, et al. Disruption of the caveolin-1 gene impairs renal calcium reabsorption and leads to hypercalciuria and urolithiasis. *Am J Pathol*. 2003;162:1241–1248.

27. Oliveira SDS, Castellon M, Chen J, et al. Inflammation-induced caveolin-1 and BMPRII depletion promotes endothelial dysfunction and TGF-beta-driven pulmonary vascular remodeling. *Am J Physiol Lung Cell Mol Physiol*. 2017;312:L760–L771.

28. Li W, Liu H, Zhou JS, et al. Caveolin-1 inhibits expression of antioxidant enzymes through direct interaction with nuclear erythroid 2 p45-related factor-2 (Nrf2). *J Biol Chem*. 2012;287:20922–20930.

29. Gu X, Reagan A, Yen A, Bhatti F, Cohen AW, Elliott MH. Spatial and temporal localization of caveolin-1 protein in the developing retina. *Adv Exp Med Biol*. 2014;801:15–21.

30. Prusky GT, Alam NM, Beekman S, Douglas RM. Rapid quantification of adult and developing mouse spatial vision using a virtual optomotor system. *Invest Ophthalmol Vis Sci*. 2004;45:4611–4616.

31. Mandal MN, Moiseyev GP, Elliott MH, et al. Alpha-phenyl-N-tert-butylnitrone (PBN) prevents light-induced degeneration of the retina by inhibiting RPE65 protein isomerohydrolase activity. *J Biol Chem*. 2011;286:32491–32501.

32. Perez-Riverol Y, Csordas A, Bai J, et al. The PRIDE database and related tools and resources in 2019: improving support for quantification data. *Nucleic Acids Res*. 2019;47:D442–D450.

33. Szklarczyk D, Franceschini A, Wyder S, et al. STRING v10: protein-protein interaction networks, integrated over the tree of life. *Nucleic Acids Res*. 2015;43:D447–D452.

34. Shannon P, Markiel A, Ozier O, et al. Cytoscape: a software environment for integrated models of biomolecular interaction networks. *Genome Res*. 2003;13:2498–2504.

35. Ge SX, Jung D, Yao R. ShinyGO: a graphical gene-set enrichment tool for animals and plants. *Bioinformatics*. 2020;36:2628–2629.

36. Rosenbaum JT, Woods A, Kezic J, Planck SR, Rosenzweig HL. Contrasting ocular effects of local versus systemic endotoxin. *Invest Ophthalmol Vis Sci*. 2011;52:6472–6477.

37. Wuest TR, Carr DJ. Dysregulation of CXCR3 signaling due to CXCL10 deficiency impairs the antiviral response to herpes simplex virus 1 infection. *J Immunol*. 2008;181:7985–7993.

38. Arora M, Poe SL, Oriss TB, et al. TLR4/MyD88-induced CD11b+Gr-1 int F4/80+ non-migratory myeloid cells suppress Th2 effector function in the lung. *Mucosal Immunol*. 2010;3:578–593.

39. Rowan S, Cepko CL. Genetic analysis of the homeodomain transcription factor Chx10 in the retina using a novel multifunctional BAC transgenic mouse reporter. *Dev Biol*. 2004;271:388–402.

40. Cepko C. Intrinsically different retinal progenitor cells produce specific types of progeny. *Nat Rev Neurosci*. 2014;15:615–627.

41. Li X, McClellan ME, Tanito M, et al. Loss of caveolin-1 impairs retinal function due to disturbance of subretinal microenvironment. *J Biol Chem*. 2012;287:16424–16434.

42. Lakk M, Yarishkin O, Baumann JM, Iuso A, Krizaj D. Cholesterol regulates polymodal sensory transduction in Muller glia. *Glia*. 2017;65:2038–2050.

43. Elliott MH, Fliesler SJ, Ghalayini AJ. Cholesterol-dependent association of caveolin-1 with the transducin alpha subunit in bovine photoreceptor rod outer segments: disruption by cyclodextrin and guanosine 5'-O-(3-thiotriphosphate). *Biochemistry*. 2003;42:7892–7903.

44. Lajoie P, Goetz JG, Dennis JW, Nabi IR. Lattices, rafts, and scaffolds: domain regulation of receptor signaling at the plasma membrane. *J Cell Biol*. 2009;185:381–385.

45. Bishop GA. TRAF3 as a powerful and multitalented regulator of lymphocyte functions. *J Leukoc Biol*. 2016;100:919–926.

46. Hauer J, Puschner S, Ramakrishnan P, et al. TNF receptor (TNFR)-associated factor (TRAF) 3 serves as an inhibitor

of TRAF2/5-mediated activation of the noncanonical NF-kappaB pathway by TRAF-binding TNFRs. *Proc Natl Acad Sci USA*. 2005;102:2874–2879.

47. He JQ, Saha SK, Kang JR, Zarnegar B, Cheng G. Specificity of TRAF3 in its negative regulation of the noncanonical NF-kappa B pathway. *J Biol Chem*. 2007;282:3688–3694.

48. Hacker H, Tseng PH, Karin M. Expanding TRAF function: TRAF3 as a tri-faced immune regulator. *Nat Rev Immunol*. 2011;11:457–468.

49. Hao Q, Jiao S, Shi Z, et al. A non-canonical role of the p97 complex in RIG-I antiviral signaling. *EMBO J*. 2015;34:2903–2920.

50. Tseng PH, Matsuzawa A, Zhang W, Mino T, Vignali DA, Karin M. Different modes of ubiquitination of the adaptor TRAF3 selectively activate the expression of type I interferons and proinflammatory cytokines. *Nat Immunol*. 2010;11:70–75.

51. Fang DF, He K, Wang N, et al. NEDD4 ubiquitinates TRAF3 to promote CD40-mediated AKT activation. *Nat Commun*. 2014;5:4513.

52. Payne S, De Val S, Neal A. Endothelial-Specific Cre Mouse Models. *Arterioscler Thromb Vasc Biol*. 2018;38:2550–2561.

53. De Ieso ML, Gurley JM, McClellan ME, et al. Physiologic Consequences of Caveolin-1 Ablation in Conventional Outflow Endothelia. *Invest Ophthalmol Vis Sci*. 2020;61:32.

54. Ito A, Shiroto T, Godo S, et al. Important roles of endothelial caveolin-1 in endothelium-dependent hyperpolarization and ischemic angiogenesis in mice. *Am J Physiol Heart Circ Physiol*. 2019;316:H900–H910.

55. Saito H, Godo S, Sato S, et al. Important Role of Endothelial Caveolin-1 in the Protective Role of Endothelium-dependent Hyperpolarization Against Nitric Oxide-Mediated Nitrative Stress in Microcirculation in Mice. *J Cardiovasc Pharmacol*. 2018;71:113–126.

56. O'Koren EG, Mathew R, Saban DR. Fate mapping reveals that microglia and recruited monocyte-derived macrophages are definitively distinguishable by phenotype in the retina. *Sci Rep*. 2016;6:20636.

57. Moseman EA, Blanchard AC, Nayak D, McGavern DB. T cell engagement of cross-presenting microglia protects the brain from a nasal virus infection. *Sci Immunol*. 2020;5:eabb1817.

58. Dunay IR, Damatta RA, Fux B, et al. Gr1(+) inflammatory monocytes are required for mucosal resistance to the pathogen Toxoplasma gondii. *Immunity*. 2008;29:306–317.

59. Getts DR, Terry RL, Getts MT, et al. Ly6c+ "inflammatory monocytes" are microglial precursors recruited in a pathogenic manner in West Nile virus encephalitis. *J Exp Med*. 2008;205:2319–2337.

60. Li Q, Lan X, Han X, Wang J. Expression of Tmem119/Sall1 and Ccr2/CD69 in FACS-Sorted Microglia- and Monocyte/Macrophage-Enriched Cell Populations After Intracerebral Hemorrhage. *Front Cell Neurosci*. 2018;12:520.

61. Pennati A, Nylen EA, Duncan ID, Galipeau J. Regulatory B Cells Normalize CNS Myeloid Cell Content in a Mouse Model of Multiple Sclerosis and Promote Oligodendrogenesis and Remyelination. *J Neurosci*. 2020;40:5105–5115.

62. McPherson SW, Heuss ND, Lehmann U, Roehrich H, Abedin M, Gregerson DS. The retinal environment induces microglia-like properties in recruited myeloid cells. *J Neuroinflammation*. 2019;16:151.

63. Dillon CP, Balachandran S. StIKKing it to a death kinase: IKKs prevent TNF-alpha-induced cell death by phosphorylating RIPK1. *Cytokine*. 2016;78:47–50.

64. Vy Tran AH, Hahm SH, Han SH, Chung JH, Park GT, Han YS. Functional interaction between hMYH and hTRADD in the TNF-alpha-mediated survival and death pathways of HeLa cells. *Mutat Res*. 2015;777:11–19.

65. Wang K, Zhu X, Mei D, Ding Z. Caveolin-1 contributes to anoikis resistance in human gastric cancer SGC-7901 cells via regulating Src-dependent EGFR-ITGB1 signaling. *J Biochem Mol Toxicol*. 2018;32:e22202.

66. Tang W, Feng X, Zhang S, et al. Caveolin-1 Confers Resistance of Hepatoma Cells to Anoikis by Activating IGF-1 Pathway. *Cell Physiol Biochem*. 2015;36:1223–1236.

67. de Hoz R, Rojas B, Ramirez AI, et al. Retinal Macroglial Responses in Health and Disease. *Biomed Res Int*. 2016;2016:2954721.

68. Kumar A, Shamsuddin N. Retinal Muller glia initiate innate response to infectious stimuli via toll-like receptor signaling. *PLoS One*. 2012;7:e29830.

69. Rutar M, Natoli R, Chia RX, Valter K, Provis JM. Chemokine-mediated inflammation in the degenerating retina is coordinated by Muller cells, activated microglia, and retinal pigment epithelium. *J Neuroinflammation*. 2015;12:8.

70. Moon H, Lee CS, Inder KL, et al. PTRF/cavin-1 neutralizes non-caveolar caveolin-1 microdomains in prostate cancer. *Oncogene*. 2014;33:3561–3570.

71. Inder KL, Ruelcke JE, Petelin L, et al. Cavin-1/PTRF alters prostate cancer cell-derived extracellular vesicle content and internalization to attenuate extracellular vesicle-mediated osteoclastogenesis and osteoblast proliferation. *J Extracell Vesicles*. 2014;3:10.3402/jev.v3.23784.

72. Wang M, Wong WT. Microglia-Muller cell interactions in the retina. *Adv Exp Med Biol*. 2014;801:333–338.

73. Wang M, Ma W, Zhao L, Fariss RN, Wong WT. Adaptive Muller cell responses to microglial activation mediate neuroprotection and coordinate inflammation in the retina. *J Neuroinflammation*. 2011;8:173.

74. Fontainhas AM, Wang M, Liang KJ, et al. Microglial morphology and dynamic behavior is regulated by ionotropic glutamatergic and GABAergic neurotransmission. *PLoS One*. 2011;6:e15973.

75. Wajant H, Henkler F, Scheurich P. The TNF-receptor-associated factor family: scaffold molecules for cytokine receptors, kinases and their regulators. *Cell Signal*. 2001;13:389–400.

76. Gurley JM, Elliott MH. The Role of Caveolin-1 in Retinal Inflammation. *Adv Exp Med Biol*. 2019;1185:169–173.